Journal of Superconductivity and Novel Magnetism
https://doi.org/10.1007/s10948-024-06754-1

RESEARCH

Ab Initio Prediction of the Structural, Elastic and Thermodynamic Properties Under Hydrostatic Pressure of the Ternary Tetragonal Phosphides XRh_2P_2 (X = Ca, Ba) for Superconducting Application

Maamar Slimani[1] · Missoum Radjai[2] · Abdelmadjid Bouhemadou[3] · Yousf Islem Bourezg[1] · Sarah Chaba Mouna[2] · Saad Bin-Omran[4]

Received: 6 January 2024 / Accepted: 24 April 2024

Abstract
This study uses density functional theory calculations to study the impact of pressure on the structural, elastic, and thermodynamic properties of $CaRh_2P_2$ and $BaRh_2P_2$ compounds. The equilibrium structural parameters closely match the experimental values. $CaRh_2P_2$ shows a greater reduction in lattice parameter "*a*" under pressure, while $BaRh_2P_2$ shows the opposite trend. The single-crystal elastic constants calculated for both compounds meet the criteria for mechanical stability under varying pressures up to 18 GPa. The study extends to polycrystalline elastic properties, including bulk modulus, shear modulus, Young's modulus, Poisson's ratio, and related properties, under pressures up to 18 GPa. The Pugh ratio, Cauchy pressure, and Poisson's ratio indicate the ductile behavior of the title compounds. $BaRh_2P_2$ exhibits superconducting characteristics, unlike $CaRh_2P_2$, confirmed by interlayer PP bond length calculations. Debye's quasi-harmonic model explores the temperature dependencies of various properties, with results that align well with elastic constant data, thus validating the results.

Keywords Ternary rhodium phosphides · DFT calculations · Elastic moduli · Pressure effect · Thermodynamic properties · Minimum thermal conductivities

1 Introduction

Advancements in modern technology and industry have seen an increasing reliance on superconducting materials in recent years. Notably, the discovery of high-temperature superconductors in 1986 sparked a revolutionary transformation, opening up possibilities for practical applications in diverse fields, including energy transfer, energy storage, and medical imaging [1, 2]. Among these materials, layered ternary intermetallic compounds with the $ThCr_2Si_2$-type (also known as 122-type) structure have been extensively investigated due to their intriguing and diverse physical phenomena [3]. Researchers have been particularly drawn to these materials because of their noteworthy properties, such as low-temperature superconductivity [4, 5], as well as the ability to exhibit high-temperature superconductivity under the influence of chemical doping and external pressure [6]. Additionally, these compounds exhibit other intriguing characteristics, such as heavy fermion behavior, unique magnetic ordering, and quantum criticality [3, 7–9]. The origins of the $ThCr_2Si_2$-type structure can be traced back to 1965 when Ban and Sikirica first reported it [10]. Subsequently, in 1996, Just and Paufler conducted an extensive geometric analysis of nearly 600 compounds with $ThCr_2Si_2$-type structure [11]. These compounds are typically represented by the chemical formula AB_2X_2, where A can be alkali, alkaline earth, or rare earth metals, B represents transition

✉ Missoum Radjai
mradjai@yahoo.com

1 Physico-chemistry of Materials and Environment Laboratory, Ziane Achour University of Djelfa, Djelfa, BP 3117, Algeria

2 Laboratory of Physics of Experimental Techniques and Their Applications (LPTEAM), University Yahia Fares, Medea, Algeria

3 Laboratory for Developing New Materials and their Characterizations, Department of Physics, Faculty of Sciences, Ferhat Abbas University – Setif 1, 19000 Setif, Algeria

4 Department of Physics and Astronomy, College of Science, King Saud University, P.O. Box 2455, Riyadh 11451, Saudi Arabia

Published online: 10 May 2024

metals, and X includes elements from groups 13 to 15 of the periodic table [12, 13]. The 122-type ternary compounds exist in two distinct structures, depending on temperature conditions. The first structure, with a primitive tetragonal arrangement, is exemplified by $CaBe_2Ge_2$ (space group P4/nmm). The second structure, characterized by a body-centered tetragonal arrangement, is represented by $ThCr_2Si_2$ (space group I4/mmm) [14]. The $ThCr_2Si_2$-type structure corresponds to space group I4/mmm (no. 139) and has been identified in over seven hundred compounds [15]. The synthesis of iron-based superconductors with $ThCr_2Si_2$-type structure, such as AFe_2As_2 (A = Ca, Ba, Sr, Eu), showcasing high critical temperatures of up to 49 K, marked a remarkable breakthrough and played a pivotal role in advancing current technology [16]. However, due to challenges in manufacturing iron-based superconducting materials, researchers have directed their efforts toward exploring alternative ternary intermetallic $ThCr_2Si_2$-type materials with promising superconducting properties.

Hoffmann and Zheng [17] performed band structure calculations to elucidate the bonding and anti-bonding characteristics of the interlayer P-P bond in the $ThCr_2Si_2$ structure, which explains the noticeable variation in bond length. The length of the interlayer P-P bond has been identified as a crucial factor in the occurrence of superconductivity in the 122-type phosphides [18]. Theoretical considerations propose a critical interlayer P-P bond length of approximately 2.8 Å ($d_{P-P} \approx 2.8$ Å) for the formation of a covalent bond. Hence, to achieve a superconducting compound within the 122-type series, the interlayer P-P bond length needs to be greater than 2.8 Å [19]. Due to their intriguing superconductive properties at remarkably low temperatures (Tc below 3 K), $ThCr_2Si_2$-type compounds, such as $CaPd_2Ge_2$ (Tc = 1.98 K) [20], $BaNi_2P_2$ (Tc ≈ 3.0 K) [21], YIr_2Si_2 (Tc = 2.52 K) [22], $BaIr_2P_2$ (Tc = 2.1 K), $BaRh_2P_2$ (Tc = 1.0 K) [23], have attracted significant interest from researchers. It is evident that 122-type superconducting materials have played a crucial role in the advancement of modern technology. Therefore, the primary objective of this current study is to explore some fundamental physical properties of superconducting materials XRh_2P_2 (X = Ba, Ca). To achieve this, we have conducted ab initio calculations through the Density Functional Theory (DFT)-based pseudopotential plane wave (PP-PW) method. These calculations aim to determine the structural, elastic, and thermodynamic properties of the ternary phosphides $BaRh_2P_2$ and $CaRh_2P_2$. The paper is structured as follows: Section 2 provides a detailed explanation of the methodology and the specific calculation parameters employed. In Section 3, we present the analysis and discussion of the physical property results obtained from the calculations. Finally, Section 4 highlights the key findings of the study.

2 Calculational Approches and Settings

Our theoretical investigation was conducted using the pseudopotential plane wave (PP-PW) approach based on density functional theory (DFT) as implemented in the CASTEP program [24]. The exchange-correlation interactions were described using the PBEsol version of the generalized gradient approximation, known as GGA-PBEsol [25]. To model the Coulomb interactions between valence electrons (Ba-$5s^25p^66s^2$, Rh-$4d^85s^1$, P-$3s23p^3$, and Ca-$3s^23p^64s^2$) and the ionic core, Vanderbilt-type ultrasoft pseudopotentials [26] were employed. For the basis set in the plane-wave approach, cut-off energy of 610 eV was chosen for $BaRh_2P_2$ and $CaRh_2P_2$. To sample the irreducible Brillouin zone, the Monkhorst-Pack scheme [27] was utilized with a grid of $8 \times 8 \times 11$ k-points. The structural parameters were optimized using the BFGS (Broyden-Fletcher-Goldfarb-Shanno) technique [28]. Convergence tolerances were set as follows: the total energy convergence was within the limit of $5.06 \times 10^{-6} eV/atom$, the maximum Hellmann–Feynman force is within the limit of 0.01 eV / $\AA$, the maximum displacement is within the limit of 5.0×10^{-4} $\AA$, and the maximum stress is within the limit of 0.02 GPa. The elastic constants (denoted as C_{ij}) are ascertained through the meticulous execution of two distinct and specialized modes of finite lattice distortions. By subjecting the lattice to these deliberate deformations, the resultant strain-stress linear relationship is diligently analyzed and subsequently employed as the foundational basis for the derivation of the elastic constants [29]. Temperature and pressure dependencies of certain macroscopic thermodynamic parameters, such isobaric and isochoric heat capacities, thermal volume expansion coefficient and Debye temperature, of the studied materials were explored using the quasi-harmonic Debye model implemented in the GIBBS program [30].

3 Results and Discussion

3.1 Structural Properties

$CaRh_2P_2$ and $BaRh_2P_2$ materials adopt a tetragonal crystal structure known as the $ThCr_2Si_2$-type, characterized by the space group I4/mmm (No. 139) [31]. In the conventional unit cell (shown in Fig. 1), there are two formula units, housing a total of 10 atoms, while the primitive unit cell contains only one chemical formula, consisting of five atoms. The positions of these atoms are as follows: Ca (or Ba) atoms occupy the 2a site at coordinates (0,0,0), Rh atoms occupy the 4d site at coordinates (0,1/2,1/4), and P atoms are located at the 4e site with coordinates (0,0,z_P).

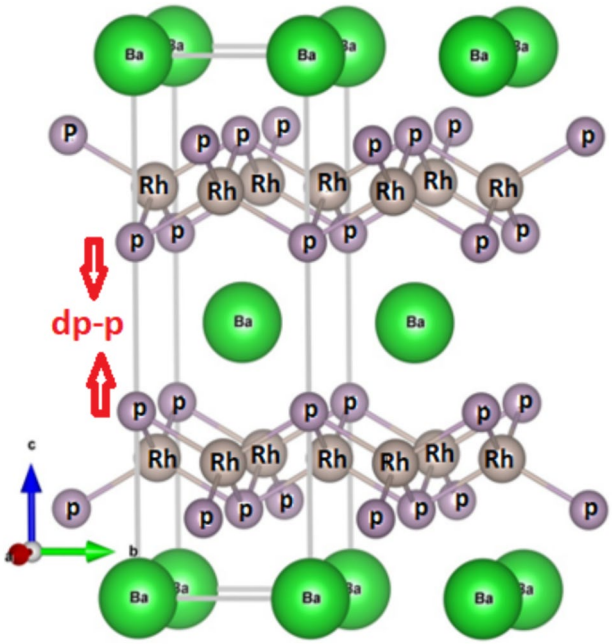

Fig. 1 The tetragonal unit cell of $BaRh_2P_2$ crystal. The $BaRh_2P_2$ structure can be viewed alternating layers of RhP connected via the Ba atom. d_{P-P} is the length of the interlayer P-P bond

The internal parameter z_P determines the z-coordinate of the P atom in the unit cell [18, 31]. The crystal structures of $CaRh_2P_2$ and $BaRh_2P_2$ can be conceptualized as alternating infinite layers. These layers consist of Rh atoms bonded with P atoms, forming RhP chains that are stacked along the crystallographic *c*-axis, the longest axis of the tetragonal lattice. These RhP chains are separated by the Ca (or Ba) atoms, which give rise to the overall structure. To determine the equilibrium lattice parameters a_0 and c_0, as well as the z_P fractional coordinate that correspond to the minimum total energy of the XRh_2P_2 compounds (X = Ca, Ba), all free structural parameters, namely a, *c* and z_P, have been fully relaxed. The resulting values for these parameters are presented in Table 1, along with previously reported values for the title compounds [18, 31] and for other compounds having the 122-type crystal structure [32–36]. The calculated equilibrium lattice parameters (a_0 and c_0) as well as the internal coordinate parameter z_P for the XRh_2P_2 compounds, where X can be Ca or Ba, closely match the experimental counterparts available in the literature [18, 31]. This congruence between the computed and experimental data enhances the reliability and validity of the computational methods used to analyze the crystal structures of these materials. Such accurate alignment between theory and experiment is of significant importance in the field of solid-state physics and materials science, as it reaffirms the precision and predictive capability of computational techniques for investigating the structural properties of complex compounds like XRh_2P_2. The volume of the unit cell of $BaRh_2P_2$ is bigger than that of $BaRh_2P_2$, with values of V = 192.51 Å^3 and V = 158.64 Å^3, respectively. The sole distinction between these two compounds lies in the Ba and Ca atoms. Consequently, the observed variation in unit cell volume can be ascribed to the higher radius of the Ba atom compared to that of the Ca atom.

The length of the interlayer P-P bond plays a crucial role in determining the occurrence of superconductivity

Table 1 Calculated equilibrium lattice parameters (a_0 and c_0, in Å), *z*-coordinate of the P atom (z_P), bulk modulus (*B*, in GPa), interlayer P-P bond length (d_{P-P}, in Å) and the enthalpies of formation (ΔH, in eV/atom) for XRh_2P_2 (X = Ca, Ba) in comparison with those of certain isostructural compounds

	a_0	c_0	c_0/a_0	z_P	*B*	d_{P-P}	ΔH
$CaRh_2P_2$							
Present	3.9802	9.649	2.424	0.384	148.2[a], 148.2[b]	2.230	-2.31
Expt. [31]	4.0180	9.660	2.404	0.383	-	-	-
Expt. [18]	4.0179	9.655	2.403	-	-	2.241	-
$BaRh_2P_2$							
Present	3.9109	12.586	3.218	0.351	91.9[a], 91.1[b]	3.712	-2.29
Expt. [31]	3.9390	12.546	3.185	0.351	-	-	-
Expt. [18]	3.9308	12.574	3.199	-	-	3.725	-
$BaRu_2P_2$							
Other [32]	4.014	11.993	2.988	0.344	88.7[a], 91.1[b]	-	-2.09
Expt. [33]	4.029	12.064	2.994	0.368	-	-	-
Expt. [34]	4.031	12.062	2.992	-	-	-	-
$CaRu_2P_2$							
Other [35]	4.029	9.641	2.392	0.369	109.8[a], 110.9[b]	-	-
Expt. [36]	4.046	9.771	2.415	-	-	-	-
Expt. [33]	4.048	9.773	2.414	0.368	-	-	-

[a]From the fit of the E–V data to Birch–Murnaghan EOS

[b]From the fit of the E–V to Vinet EOS

in 122-type phosphides [18]. This parameter, denoted as d_{P-P}, serves as an indicator of the presence or absence of interlayer P-P covalent bonds. A critical length of the interlayer P-P bond of approximately 2.8 Å ($d_{P-P} \approx 2.8$ Å) is considered essential for the formation of interlayer P-P covalent bonds, and any value of d_{P-P} greater than 2.8 Å indicates the absence of such a bond at the P-P interface, which is associated with the emergence of superconductivity. Upon calculating the interlayer P-P bond lengths for both $CaRh_2P_2$ and $BaRh_2P2$ (as listed in Table 1), interesting findings emerge. For $CaRh_2P_2$, the computed value of d_{P-P} is 2.23 Å, falling below the critical threshold of 2.8 Å. This indicates the formation of a P-P covalent bond in $CaRh_2P_2$. On the other hand, for $BaRh_2P_2$, the calculated d_{P-P} value is 3.8 Å, surpassing the critical limit. Consequently, no interlayer P-P covalent bond is formed in $BaRh_2P_2$. These results provide an explanation for the differing superconducting behaviors observed in $CaRh_2P_2$ and $BaRh_2P_2$. As the interlayer P-P covalent bond is absent in $BaRh_2P_2$ due to its larger d_{P-P} value, this compound exhibits superconductivity. In contrast, the presence of a P-P covalent bond in $CaRh_2P_2$, owing to its smaller d_{P-P} value, prevents superconductivity from occurring. It is worth to remark that the distinctive difference between $CaRh_2P_2$ and $BaRh_2P_2$ is located in the Ba and Ca atoms. Thus the fact the interlayer P-P covalent bond in $BaRh_2P_2$ is bigger than that in $CaRh_2P_2$ may be attributed the fact that the atomic radius of Ba is larger than that of Ca.

We conducted an investigation into the pressure dependencies of the unit cell volume (V) and the lattice parameters (a and c). To analyze the behavior of these parameters under varying pressure conditions, we utilized normalized values. The normalized unit cell volume (V/V_0) represents the ratio of the unit cell volume at a certain pressure (V) to its value at zero pressure (V_0). Similarly, the normalized lattice parameters, a/a_0 and c/c_0, indicate the ratios of the lattice parameters (a and c) at pressure P to their respective values at zero pressure (a_0 and c_0). Second-order polynomials were employed to fit the variations of the normalized unit cell volume (V/V_0) and the normalized lattice parameters (a/a_0 and c/c_0) under hydrostatic pressure. The fitting process allowed for a more precise representation of the relationships between the crystal lattice's structural parameters and the applied pressure as follows:

$$CaRh_2P_2\begin{cases}\dfrac{a}{a_0} = 1 - 2.35\times10^{-3}P + 2.58\times10^{-5}P^2\\ \dfrac{c}{c_0} = 1 - 1.68\times10^{-3}P + 1.86\times10^{-5}P^2\\ \dfrac{V}{V_0} = 1 - 6.33\times10^{-3}P + 7.66\times10^{-4}P^2\end{cases} \quad (1)$$

$$BaRh_2P_2\begin{cases}\dfrac{a}{a_0} = 1 - 2.27\times10^{-3}P + 3.60\times10^{-5}P^2\\ \dfrac{c}{c_0} = 1 - 5.49\times10^{-3}P + 6.44\times10^{-5}P^2\\ \dfrac{V}{V_0} = 1 - 9.92\times10^{-3}P + 1.47\times10^{-4}P^2\end{cases} \quad (2)$$

From the data presented in Fig. 2a, it is evident that as the pressure increases, the normalized structural parameters diminish. In order to quantify this behavior, linear compressibility values along the a and c directions were estimated and found to be $\beta_a = 2.35\times10^{-3}$ GPa^{-1} (2.27×10^{-3} GPa^{-1}) and $\beta_c = 1.68\times10^{-3}$ GPa^{-1} (5.49×10^{-3}GPa^{-1}) for $CaRh_2P_2$ ($BaRh_2P_2$). Further examination of the data reveals that under the influence of pressure, a distinct behavior is observed in the variation of lattice parameters "a" and "c" for the $CaRh_2P_2$ compound compared to the $BaRh_2P_2$ compound. Specifically, for the $CaRh_2P_2$ compound, the lattice parameter "a" experiences a more pronounced reduction

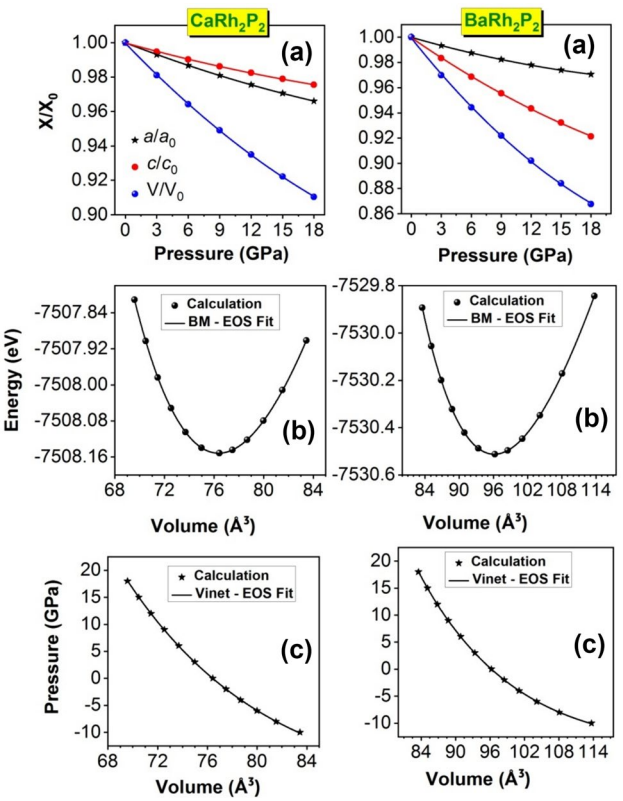

Fig. 2 **a** Pressure dependencies of a/a_0, c/c_0, and V/V_0, and **b** total energy (Energy (eV)) as function of primitive cell volume (V) and **c** hydrostatic pressure (P) as function of primitive cell volume (V) for XRh_2P_2 (X=Ca, Ba). The subscript "0" denotes the parameter value at zero pressure. The symbols are the results obtained from the first principles calculations and the solid lines are the fits. **b** fit of the E–V data to the Birch–Murnaghan (BM) EOS, and **c** fit of the P–V data to Vinet EOS

in response to applied pressure, whereas the lattice parameter "*c*" exhibits a comparatively less substantial decrease. This indicates an anisotropic response of the crystal lattice to pressure, with the "*a*" direction being more sensitive to compression compared to the "*c*" direction. In contrast, the $BaRh_2P_2$ compound demonstrates a converse trend. Here, under pressure, the lattice parameter "*c*" displays a more significant decrease compared to the lattice parameter "*a*" This signifies a differing response to pressure, with the "*c*" direction being more susceptible to compression than the "*a*" direction in this particular compound. It is important to mention that, despite the higher size of the unit cell of $BaRh_2P_2$ compared to $CaRh_2P_2$ at zero pressure, the lattice parameter "*a*" in $BaRh_2P_2$ is smaller than that in $CaRh_2P_2$, but the parameter "*c*" in $BaRh_2P_2$ is significantly larger than that in $CaRh_2P_2$. Consequently, the bond lengths along the *a*-axis in $BaRh_2P_2$ are shorter compared to those in $CaRh_2P_2$, indicating that the bonds along the *a*-axis in $BaRh_2P_2$ possess greater strength than the corresponding bonds in $CaRh_2P_2$. In contrast, the bonds along the *c*-axis in $CaRh_2P_2$ exhibit greater strength compared to the analogous bonds in $BaRh_2P_2$. The stronger the bond, the less sensitive it is to the pressure impact. This behavior may elucidate the observed inverse correlation between the lattice parameters "*a*" and "*c*" with respect to the pressure effect in $CaRh_2P_2$ and $BaRh_2P_2$.

To estimate the bulk moduli (*B*) of the XRh_2P_2 compounds, where X can be Ca or Ba, two different approaches were employed for data fitting. Firstly, the total energy versus unit cell volume (E(V)) data was fitted to the third-order Birch-Murnaghan equation of state (BM-EOS) [37]. Secondly, the hydrostatic pressure versus unit cell volume (P(V)) data was fitted to the third-order Vinet equation of state (V-EOS) [38]. These fittings are illustrated in Fig. 2b and c. The obtained bulk modulus (*B*) values are presented in Table 1. Remarkably, there was a notable agreement between the values of *B* obtained through the BM-EOS and V-EOS approaches, thus affirming the consistency and reliability of the results. It is observed that the B value of $BaRh_2P_2$ is smaller than that of $CaRh_2P_2$, which is consistent with the established relationship: $B \sim 1/V$, where V represents the unit cell volume.

To ensure the structural stability of the XRh_2P_2 compounds (where X can be either Ca or Ba), we performed an estimation of the formation enthalpy (ΔH) using a specific expression [39, 40]:

$$\Delta H = \frac{1}{n_X + n_{Rh} + n_P}\left[E_{Tot}^{XRh_2P_2} - \left(n_X E_{Tot}^{X(solid)} + n_{Rh} E_{Tot}^{Rh(solid)} + n_P E_{Tot}^{P(solid)}\right)\right] \quad (3)$$

In this context, $E_{Tot}^{XRh_2P_2}$ represents the total energy of the primitive cell of XRh_2P_2 (X = Ca, Ba), and $E_{Tot}^{X(solid)}$, $E_{Tot}^{Rh(solid)}$, and $E_{Tot}^{P(solid)}$ represent the total energies per atom of the solid state of the pure elements X (Ca or Ba), Rh, and P, respectively. n_X, n_{Rh}, and n_P are the numbers of X, Rh, and P atoms in the primitive cell, respectively. Applying this methodology, we obtained the enthalpies of formation given in Table 1 for XRh_2P_2 (X = Ca, Ba). Notably, upon examining Table 1, it becomes evident that the XRh_2P_2 compounds, whether X is Ca or Ba, exhibit negative formation enthalpies. This negative value indicates that these compounds are thermodynamically stable in their structural configuration.

3.2 Elastic Properties

3.2.1 Single-crystal Elastic Constants

Single-crystal elastic constants (C_{ij}) play a crucial role in providing essential insights into various properties of materials, such as their bonding characteristics, how they respond to external stress, their mechanical stability, and overall stiffness [41]. In addition, the elastic constants are closely related to various fundamental physical properties, such as specific heat, melting point, Debye temperature, thermal expansion coefficient. In the context of a tetragonal system, there are six independent elastic constants that are of particular importance. These constants are denoted as C_{11}, C_{12}, C_{13}, C_{33}, C_{44}, and C_{66}. Table 2 presents the values of these six elastic constants for the XRh_2P_2 (X = Ca, Ba) tetragonal systems and those of some isostructural compounds [32, 35, 42]. Comparing these values with those from other related compounds helps in understanding the similarities and differences in the properties of these materials, thus contributing to the broader understanding of their behavior and applications. We can make some observations from the calculated elastic constants in XRh_2P_2 (X = Ca, Ba) compounds:

(i) One notable observation from the calculated elastic constants (C_{ij}) in XRh_2P_2 compounds (where X = Ca, Ba) is that C_{11} (which represents the linear compression resistance along the *a*-axis) is greater than C_{33} (which characterizes the linear compression resistance along the *c*-axis) in $BaRh_2P_2$. However, in $CaRh_2P_2$, C_{11} is smaller than C_{33}. This finding suggests that the linear compressibility along the *a*-direction should be lower than that along the *c*-direction in $BaRh_2P_2$, while the opposite trend should be observed in the case of $CaRh_2P_2$. These results are consistent with the pressure dependence of lattice parameters "*a*" and "*c*" that we have already studied in Section 3.1.

(ii) The C_{ij} values show a decreasing trend from $CaRh_2P_2$ to $BaRh_2P_2$, demonstrating a decrease in C_{ij} values as the unit cell volume increases.

(iii) In the compound $BaRh_2P_2$, the value of C_{11} is greater than C_{33}. However, in the compound $CaRh_2P_2$, the value of C_{11} is smaller than C_{33}. This observation

Table 2 The calculated elastic constants (C_{ij}, in GPa), compliances constants (S_{ij}, in GPa^{-1}) and melt temperature (T_m, in K) for XRh_2P_2 (X = Ca, Ba) along with previous calculations for some isostructural compounds

Compound	C_{11}	C_{12}	C_{13}	C_{33}	C_{44}	C_{66}	T_m
$CaRh_2P_2$	239.4	91.1	108.0	261.0	79.4	100.2	1463.7
$BaRh_2P_2$	188.1	73.2	57.7	119.0	37.9	100.3	1096.8
$BaRu_2P_2$ [32]	216.9	93.8	57.9	99.3	39.7	117.7	1153.8
$BaRu_2As_2$ [32]	179.3	74.1	57.4	89.89	37.7	85.6	1026.9
$CaRu_2As_2$ [35]	237.6	90.9	63.4	100.9	47.3	100.9	1026.9
$CaRu_2P_2$ [35]	314.6	58.3	116.2	149.9	79.6	152.1	1276.2
YRu_2P_2 [42]	309.3	114.9	85.3	220.4	85.8	141.8	1612.5
S_{ij}	S_{11}	S_{12}	S_{13}	S_{33}	S_{44}	S_{66}	
$CaRh_2P_2$	0.0054456	-0.0012981	-0.0017164	0.0052200	0.0125997	00.0099752	
$BaRh_2P_2$	0.0067858	-0.0019179	-0.0023593	0.0106908	0.0263541	0.0099688	
$BaRu_2P_2$ [32]	0.0061117	-0.0020088	-0.0023830	0.0128360	0.0252083	0.0085033	
$BaRu_2As_2$ [32]	0.0075274	-0.0019751	-0.0035467	0.0156551	0.0265424	0.0116876	
$CaRu_2As_2$ [35]	0.0052522	-0.0015616	-0.0016734	0.0086791	0.0211648	0.0099171	
$CaRu_2P_2$ [35]	0.0038241	-0.0012275	-0.0010091	0.0074550	0.0125669	0.0065736	

aligns with the controversies responses of "*a*" and "*c*" to changes in pressure in $CaRh_2P_2$ and $BaRh_2P_2$, as stated in Section 3.1.

(iv) Another significant observation pertains to C_{44}, which characterizes the material's resistance against shear distortion in the (100) plane, and C_{66}, which characterizes the resistance to shear in the <110> direction. The calculated values indicate that C_{44} is greater than C_{66}, suggesting that XRh_2P_2 compounds (X = Ca, Ba) are more competent in resisting shear distortion along the <110> direction compared to the (100) plane [43].

(v) The elastic constants C_{11} and C_{33} are somewhat larger than C_{44} and C_{66}. This finding implies that XRh_2P_2 compounds (X = Ca, Ba) should be more resistant to unidirectional compression than to shear deformation.

(vi) The Cauchy pressure (C_{12}–C_{44}) is an important indicator of material ductility or brittleness. When the Cauchy pressure is negative, the material tends to be brittle, whereas a positive value indicates ductility [43]. In the case of both XRh_2P_2 compounds (X = Ca, Ba), the Cauchy pressure (C_{12}–C_{44}) is positive, indicating that they are ductile materials.

(vii) The linear compressibility along the *a*-direction (β_a) and *c*-direction (β_c) in a tetragonal crystal can be represented as follows [44]: $\beta_a = S_{11} + S_{12} + S_{13}$, and $\beta_c = S_{33} + 2S_{13}$, where S_{ij} are the compliance constants The calculated values of β_a and β_c for $CaRh_2P_2$ ($BaRh_2P_2$) are found to be 2.4×10^{-3} GPa^{-1} (2.5×10^{-3} GPa^{-1}) and 1.7×10^{-3} GPa^{-1} (5.9×10^{-3} GPa^{-1}), respectively. These values are very close to the linear compressibilities obtained from the pressure dependence of the lattice parameters *a* and *c* studied in Section 3.1, and reflect well the fact that the linear compressibility along the *a*-direction is greater than that along the along the *c*-direction in $CaRh_2P_2$, while the compound $BaRh_2P_2$ exhibits an opposite trend. This close agreement supports the reliability of the calculated elastic constants.

(viii) It is interesting to note that the values of the elastic constants (C_{ij}) increase when the Ba atom in $BaRh_2P_2$ is replaced by the Ca atom, leading to a decrease in stiffness when transitioning from $CaRh_2P_2$ to $BaRh_2P_2$.

(ix) In the realm of materials science, the critical parameter known as the melting temperature (T_m) assumes considerable significance, as it defines the temperature at which a given material undergoes a transformative shift from its solid state to a liquid state. The quantification of this pivotal parameter can be accomplished through the application of the following mathematical relationship [45]:

$$T_m = 354 + [4.5(2C_{11} + C_{33})/3] \quad (4)$$

The computed values od T_m for the considered compounds are presented in Table 2.

(x) Lastly, it is crucial to consider the mechanical stability requirements at zero pressure. In this regard, the calculated values of the single-crystal elastic constants satisfy the required conditions for mechanical stability [46]:

$$C_{11} > 0;\ C_{33} > 0;\ C_{44} > 0;\ C_{66} > 0;\ C_{11} + C_{33} - 2C_{13} > 0;$$
$$C_{11} - C_{12} > 0;\ 2(C_{11} + C_{12}) + 4C_{13} + C_{33} > 0 \quad (5)$$

His indicates the mechanical stability of the XRh_2P_2 (X = Ca, Ba) compounds.

The graph presented in Fig. 3 illustrates the variations of C_{ij} as a function of pressure within the range of 0 to 18 GPa. It is noteworthy that the calculated values of Cij at specific pressures (C_{ij}(P)), namely 0, 3, 6, 9, 12, 15, and 18 GPa, fulfill the necessary conditions for mechanical stability under hydrostatic pressure [47, 48]:

$$\begin{aligned}&(C_{11}-C_{12})>0;\,(C_{11}+C_{33}-2C_{13})>0;\\&C_{ii}>0;\,(2C_{11}+C_{33}+2C_{12}+4C_{13})>0\end{aligned}\tag{6}$$

In this context, $C_{\alpha\alpha}=C_{\alpha\alpha}-P\,(\alpha=1,\,2,\,3,\,4,\,5,\,6)$, $C_{12}=C_{12}+P$, and $C_{13}=C_{13}+P$. This demonstrates that the materials XRh_2P_2 (where X can be either Ca or Ba) are mechanically stable under hydrostatic pressure. Furthermore, it has been observed that C_{ij} exhibit a quadratic relationship with pressure. As the pressure increases, the elastic constants increase in accordance with the following quadratic polynomials:

$$\mathrm{CaRh_2P_2}\begin{cases}C_{11}=239.40+6.23P-0.02P^2\\C_{33}=261.00+7.83P-0.01P^2\\C_{44}=79.36+1.55P-0.01P^2\\C_{66}=100.22+4.58P-0.05P^2\\C_{12}=90.96+3.44P-0.03P^2\\C_{13}=108.08+5.20P-0.07P^2\end{cases}\tag{7}$$

$$\mathrm{BaRh_2P_2}\begin{cases}C_{11}=188.11+6.70P-1.5\times10^{-3}\,P^2\\C_{33}=118.99+5.24P-6.3\times10^{-2}\,P^2\\C_{44}=37.94+2.96P-1.9\times10^{-2}\,P^2\\C_{66}=100.30+4.27P-5.6\times10^{-2}\,P^2\\C_{12}=73.19+4.83P-3.1\times10^{-3}\,P^2\\C_{13}=57.67+3.93P-1.4\times10^{-2}\,P^2\end{cases}\tag{8}$$

3.2.2 Polycrystalline Elastic Moduli

The elastic properties of polycrystalline aggregates can be characterized by a pair of isotropic elastic moduli, namely the bulk and shear moduli (B and G). The polycrystalline bulk and shear moduli (B and G) can be determined from the single-crystal elastic constants (C_{ij}) via the Voigt-Reuss-Hill approaches [49–51]. The Reuss [49] and Voigt [50] approximations are employed to obtain the extreme values of B (B_R, B_V) and G (G_R, G_V) for polycrystalline samples. The subscript "R" or "V" serves as a denotation that the adopted approximation pertains to the Reus or Voigt approximation, correspondingly. In the case of a tetragonal system, the polycrystalline elastic moduli B_R, B_V, G_R, and G_V are expressed as functions of C_{ij} as follows [52]:

$$\begin{aligned}&B_V=\tfrac{1}{9}\left(2(C_{11}+C_{12})+C_{33}+4C_{13}\right);\\&G_V=\tfrac{1}{30}\left(M+3C_{11}-3C_{12}+12C_{44}+6C_{66}\right);\\&B_R=C^2/M;\\&G_R=15\left\{\left(\frac{18B_V}{C^2}\right)+\left[\frac{6}{(C_{11}-C_{12})}\right]+\left(\frac{6}{C_{44}}\right)+\left(\frac{3}{C_{66}}\right)\right\}^{-1}\end{aligned}\tag{9}$$

In this context, $M=(C_{11}+C_{12})+2C_{33}-44C_{13}$, and $C^2=\left(C_{11}-C_{12}\right)C_{33}-2C_{13}^2$. According to the Hill approximation, the effective values of the bulk and shear moduli (B_H and G_H) are given by the arithmetic mean of the Voigt and Reuss limits [51]:

$$B_H=\left(B_V+B_R\right)/2;\;G_H=\left(G_V+G_R\right)/2\tag{10}$$

Another pair of polycrystalline elastic moduli, namely Young's modulus (E) and Poisson's ratio (σ), can be calculated from B and G using the following relationships:

$$E=\frac{9BG}{(3B+G)};\;\sigma=\frac{(3B-2G)}{(6B+2G)}\tag{11}$$

Additionally, to quantify the hardness of a material, the Vickers hardness (H_V) is commonly used as a powerful tool to describe the hardness of solids. Chen et al. [53, 54] proposed an expression for the Vickers hardness (H_V) based on the obtained elastic moduli B and G, using the following relationship:

$$H_{\mathrm{V}}=2\left(K^2G\right)^{0.585}-3\tag{12}$$

Here, $K=G/B$. The predicted values of the polycrystalline moduli: B_V, B_R, G_V, G_R, G_H, E_H, σ_H, and H_V, for the considered tetragonal crystals XRh_2P_2 (X = Ca, Ba) are listed in Table 3. This table also includes results from the literature for certain isostructural compounds [32, 37, 42]. From the data presented in Table 3, several significant conclusions can be drawn:

(i) The bulk modulus (B) values obtained through the equation of state (EOS) fits for $CaRh_2P_2$ (B = 148.2 GPa) and $BaRh_2P_2$ (B = 91.8 GPa) closely align with those calculated from the single-crystal elastic constants, namely B = 149.6 GPa for $CaRh_2P_2$ and B = 93.9 GPa for $BaRh_2P_2$. This concordance between the two independent methods serves as strong evidence of the reliability and accuracy of the computed single elastic constants.

(ii) The determination of a material's brittleness or ductility holds considerable importance, as ductile materials are known for their ease of machinability and resilience to thermal shock. Poisson's ratio (σ) and Pugh's ratio (B/G) have proven to be effective indicators in distinguishing between ductile and brittle materials. When

Table 3 Calculated bulk and shear modulus values via Voigt approximation (B_V, G_V, in GPa), Reuss approximation (B_R, G_R, in GPa), and Hill approximation (B_H, G_H, in GPa), Hill Young's modulus (E_H, in GPa), Hill Poisson's ratio (σ_H, dimensionless), Vickers hardness (H_V, in GPa), density of mass (ρ, in g.cm^{-3}), isotropic longitudinal, transverse and average sound velocities (V_l; V_t; V_m, in m.s^{-1}), Debye temperatures (θ_D, in K), minimum thermal conductivity (K_{min}, in W.m^{-1}.K^{-1}) and melting temperature (T_m, in K) for $CaRh_2P_2$ and $BaRh_2P_2$ materials as well as available results of certain isostructural compounds

Compound	B_R	B_V	B_H	G_R	G_V	G_H	B_H/G_H	E_H	σ_H	H_V
$CaRh_2P_2$	149.6	150.4	149.6	79.3	80.6	79.9	1.87	203.7	0.27	9.4
$BaRh_2P_2$	90.9	96.9	93.9	48.1	55.6	51.9	1.80	131.5	0.27	7.0
$BaRu_2P_2$ [32]	86.8	105.7	96.3	49.3	60.9	55.1	1.74	138.9	0.25	7.8
$BaRu_2As_2$ [32]	79.5	91.8	85.6	42.4	49.5	45.9	1.84	116.9	0.27	6.0
$CaRu_2P_2$ [35]	116.1	138.2	127.2	89.0	98.6	93.8	1.4	225.9	0.20	16.9
$CaRu_2As_2$ [35]	106.8	116.6	111.7	59.3	95.6	62.4	1.8	157.8	0.26	8.3
YRu_2P_2 [42]	-	-	153.7	-	-	97.1	1.58	240.7	0.24	43.1
Compound	ρ	V_l		V_t		V_m		θ_D		K_{min}
$CaRh_2P_2$	6.68	6196.0		3458.8		3850.7		461.8		0.86
$BaRh_2P_2$	6.98	4832.2		2725.5		3031.8		336.7		0.58
$BaRu_2P_2$ [32]	6.45	5130.0		2923.4		3249.2		352.4		0.59
$BaRu_2As_2$ [32]	7.81	4336.2		2424.9		2699.4		292.2		0.49
$CaRu_2P_2$ [35]	6.45	6252.2		3812.9		4211.2		501.1		0.85
$CaRu_2As_2$ [35]	7.35	5147.4		2912.8		3239.3		369.9		0.61
YRu_2P_2 [42]	7.40	6180		3620		928		110		0.21

Poisson's ratio is higher (or lower) than 0.26, the material is identified as ductile (or brittle) [43]. Similarly, if the B/G ratio exceeds (or is lower than) 1.75, the material exhibits ductile (or brittle) behavior [55, 56]. Based on the values listed in Table 3, it is evident that both $CaRh_2P_2$ and $BaRh_2P_2$ possess Poisson's ratios greater than 0.26 and Pugh's ratios larger than 1.75, pointing out their ductile behavior across various pressures (0, 3, 6, 9, and 18 GPa).

(iii) A comparative analysis of the bulk modulus (B), shear modulus (G), and Young's modulus (E) between $CaRh_2P_2$ and $BaRh_2P_2$ reveals that the values of aforementioned elastic moduli of $CaRh_2P_2$ are consistently higher than those of $BaRh_2P_2$. This suggests that $CaRh_2P_2$ exhibits greater resistance to deformations, implying that the chemical bonds in $CaRh_2P_2$ possess a degree of strength superior to those in $BaRh_2P_2$.

(iv) The Vickers hardness (H_V) value in $CaRh_2P_2$ surpasses that of $BaRh_2P_2$, providing concrete evidence that $CaRh_2P_2$ possesses a higher hardness level than $BaRh_2P_2$.

(v) Isotropic sound wave velocities, specifically the longitudinal, transverse, and mean sound wave velocities (denoted as V_L, V_T, and V_m), are fundamental and noteworthy physical parameters due to their intricate interrelation with various thermodynamic properties. These properties encompass the Debye temperature, thermal conductivity, heat capacity, and melting temperature. The quantities V_L, V_T, and V_m can be evaluated through explicit formulations using the isotropic bulk and shear moduli (designated as B and G, respectively), as articulated below:

$$V_T = \left(\frac{G}{\rho}\right)^{1/2}; V_L = \left(\frac{3B+4G}{3\rho}\right)^{1/2}; V_m = \left[\frac{1}{3}\left(V_L^{-3} + 2V_T^{-3}\right)\right]^{-1/3} \quad (13)$$

The mass density ρ plays a pivotal role. The resulting V_L, V_T, and V_m values for the materials under scrutiny are documented within Table 3. The Debye temperature (symbolized as θ_D), an imperative thermodynamic parameter, is amenable to computation via the average sound wave velocity (V_m) in accordance with the ensuing expression [57–59]:

$$\theta_D = \frac{h}{k_B}\left[\frac{3n}{4\pi}\frac{N_A\rho}{M}\right]^{1/3} V_m \quad (14)$$

Here, the constants h, N_A, k_B, M, and n embody the Planck constant, Avogadro number, Boltzmann constant, molecular weight, and the count of atoms within the molecule, respectively. The computed θ_D values for the compounds of interest are thoughtfully juxtaposed with those belonging to some isostructural compounds [32, 35, 42], within the tabular arrangement denoted as Table 3. In the endeavor to comprehend the efficacy of heat propagation within materials, the parameter of thermal conductivity denoted as K_{min} assumes paramount importance. This parameter's significance is underscored by its intimate and

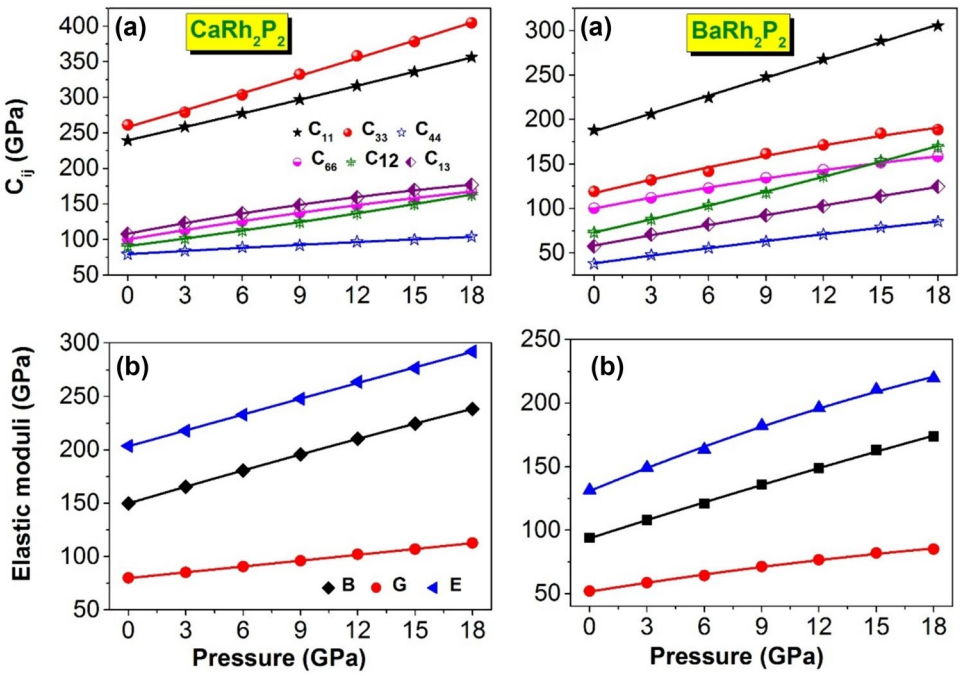

Fig. 3 Pressure-dependence of the single-crystal elastic constants (C_{ij}), and polycrystalline elastic moduli: isotropic bulk modulus B_H, shear modulus G_H, Young's modulus E_H for $CaRh_2P_2$ and $BaRh_2P_2$. The symbols are the calculated results, while the lines represent the fit curves

direct correlation with high-temperature materials [60]. The lattice thermal conductivity K_{min} for the XRh_2P_2 compounds where X stands for Ca and Ba has been calculated utilizing an established relationship [61]:

$$K_{\min} = k_B V_m \left(M/n\rho N_A\right)^{-2/3} \tag{15}$$

The plot shown in Fig. 3 illustrates the changes in polycrystalline elastic moduli, including bulk modulus (B_H), shear modulus (G_H), and Young's modulus (E_H), for both $CaRh_2P_2$ and $BaRh_2P_2$ as a function of applied pressure. To describe the relationship between these moduli and pressure, second-order polynomial equations were employed, which resulted in good fits to the calculated data. These polynomial equations effectively capture the variations of the moduli with increasing pressure.

$$CaRh_2P_2\begin{cases} B = 149.6 + 5.26P - 1.82\times10^{-2}\,P^2 \\ G = 79.9 + 1.81P - 3.26\times10^{-2}\,P^2 \\ E = 203.46 + 4.99P - 3.91\times10^{-3}\,P^2 \end{cases} \tag{16}$$

$$BaRh_2P_2\begin{cases} B = 93.9 + 4.83P - 1.89\times10^{-2}\,P^2 \\ G = 51.9 + 2.42P - 2.96\times10^{-2}\,P^2 \\ E = 131.5 + 6.25P - 6.9\times10^{-2}\,P^2 \end{cases} \tag{17}$$

Figure 4 shows that in the case of both examined compounds there exists a nearly linear augmentation of the longitudinal (V_L), transversal (V_T) and average (V_m) sound wave velocities with a rise in pressure. The alterations in V_L, V_T, and V_m exhibit a strong conformity with the mathematical representation of second-order polynomial equations:

$$CaRh_2P_2\begin{cases} V_t = 3458.8 + 27.64P - 0.11P^2 \\ V_l = 6196.0 + 70.57P - 0.58P^2 \\ V_m = 3850 + 31.79P - 0.14P^2 \end{cases} \tag{18}$$

$$BaRh_2P_2\begin{cases} V_t = 2725.5 + 45.5P - 0.86P^2 \\ V_l = 4832.2 + 87.7P - 1.30P^2 \\ V_m = 3031.8 + 51.0P - 0.95P^2 \end{cases} \tag{19}$$

The impact of pressure on key thermodynamic properties, namely the melting temperature (T_m), minimum thermal conductivity (K_{min}), and Debye temperature (θ_D), for the compounds $CaRh_2P_2$ and $BaRh_2P_2$ is illustrated in Fig. 4. It is evident that these entire aforementioned parameters exhibit a consistent upward trend as pressure is incrementally augmented. The discernment is reinforced by the data in Table 3, wherein the Debye temperature for $BaRh_2P_2$ is notably lower compared to that of $CaRh_2P_2$. This discrepancy can be attributed to the inherent mechanical rigidity disparity between the two compounds, with $CaRh_2P_2$ demonstrating greater stiffness in comparison to $BaRh_2P_2$. The resultant polynomial expressions that represent the relationships for melting temperature (Tm), minimum thermal conductivity (Kmin), and Debye temperature (θD) pertaining to the XRh_2P_2 (X = Ca, Ba) compounds are enumerated as follows:

$$\mathrm{CaRh_2P_2}\begin{cases}\theta_D = 461.8 + 4.82P - 0.02P^2\\ K_{\min} = 0.86 + 0.01P - 4.76\times10^{-5}\ P^2\\ T_m = 1463.7 + 30.44P - 0.07P^2\end{cases} \quad (20)$$

$$\mathrm{BaRh_2P_2}\begin{cases}\theta_D = 336.7 + 6.89P - 0.11P^2\\ K_{\min} = 0.58 + 1.4\times10^{-2}\ P - 2.06\times10^{-4}\ P^2\\ T_m = 1096.8 + 27.69P - 0.09P^2\end{cases} \quad (21)$$

3.2.3 Elastic Anisotropy

The assessment of elastic anisotropy in crystals holds paramount significance due to its intimate relationship with various phenomena and material properties. Notably, it plays a pivotal role in understanding the development of plastic deformation in crystals [62], the stability and configuration of dislocations in materials, the texture of nanoscale shape-memory alloys [63], and the initiation of microcracks [64]. To quantitatively estimate the extent of elastic anisotropy in crystals, several metrics have been developed. In our study, we employed four distinct metrics to estimate the degree of elastic anisotropy exhibited by the compounds under investigation. By utilizing these metrics, we aim to gain comprehensive insights into the anisotropic behavior of the studied materials.

(i) The evaluation of elastic anisotropy in crystals commonly relies on the calculation of percent anisotropy in shear ($A_{Shear} = \frac{G_V - G_R}{G_V + G_R} \times 100$) and compression ($A_{Comp} = \frac{B_V - B_R}{B_V + B_R} \times 100$) [65, 66]. Specifically, A_{Shear} is defined as the ratio of shear modulus (G), while A_{Comp} is the ratio of bulk modulus (B). These metrics serve as useful measures to quantify the extent of anisotropy in shear and compression within a crystal structure. The degree of anisotropy in shear and compression is reflected by the deviation of A_{Shear} and A_{Comp}, respectively, from zero. Higher values of A_{Shear} or A_{Comp} indicate a more pronounced anisotropic behavior, while values closer to zero imply a more isotropic crystal. In Table 4, we present the calculated values of A_{Shear} and A_{Comp} for the studied tetragonal XRh_2P_2 (X = Ca, Ba) compounds. It is evident from these results that these materials exhibit a notable degree of anisotropy in shear and compression. This finding highlights the structural anisotropy in these crystals.

(ii) To investigate the elastic anisotropy in crystals, researchers often employ the universal anisotropic index, denoted as A^U, which is defined as $A^U = 5\frac{G_V}{G_R} + \frac{B_V}{B_R} - 6$ [67, 68]. This index serves as a valuable metric for quantifying the degree of elastic anisotropy in a crystal structure. For isotropic crystals, the universal index equals zero, signifying a balanced distribution of elastic properties in all direc-

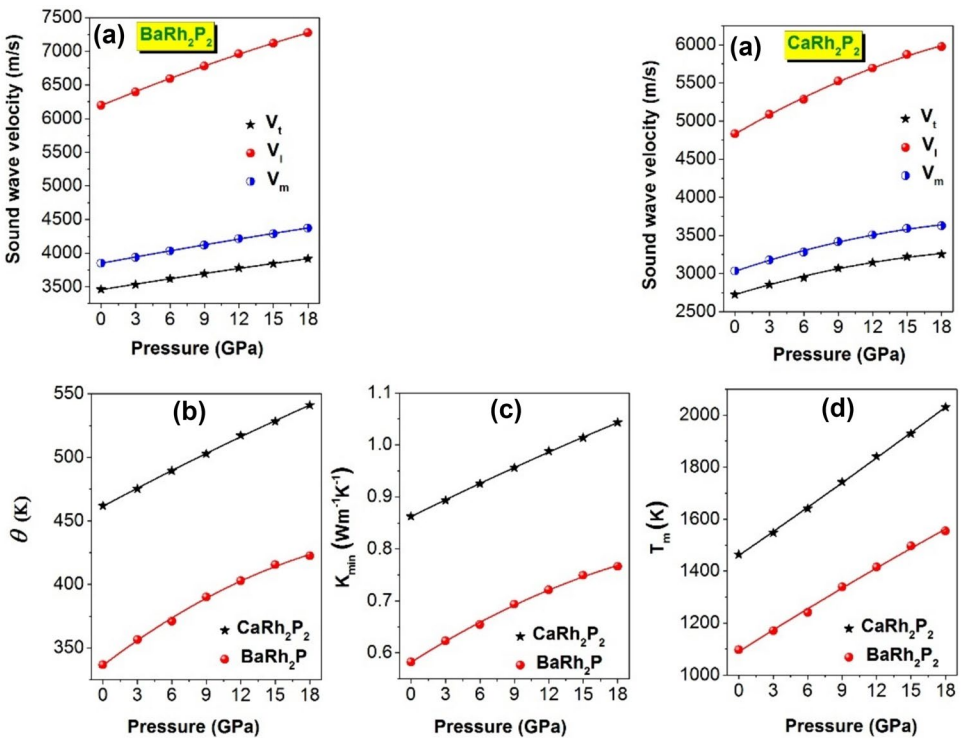

Fig. 4 Calculated pressure-dependence of the transverse, longitudinal and average sound wave velocities (V_t, V_l and V_m) (**a**), Debye temperature (θ_D) (**b**), minimum thermal conductivity (K_{min}) (**c**), and melting temperature (T_m) (**d**) for $CaRh_2P_2$ and $BaRh_2P_2$. The symbols are the calculated results, while the lines represent the fit curves

tions. However, for anisotropic crystals, the index deviates from zero, indicating the presence of varying degrees of anisotropy in the material's response to shear and compression. In Table 4, we present the calculated values of the universal anisotropic index for the studied tetragonal XRh_2P_2 (X = Ca, Ba) compounds. The results confirm the presence of strong elastic anisotropy in both materials. This finding underscores the significant variation in their elastic properties along different crystallographic directions.

(iii) The assessment of shear anisotropy factors A_1 ($A_1 = A_{\{100\}} = 4C_{44}/(C_{11} + C_{33} - 2C_{13})$) along the {100} shear planes and A_3 ($A_3 = A_{\{001\}} = 2C_{66}/(C_{11} - C_{12})$) along the {001} shear planes [69, 70] plays a crucial role in evaluating the degree of anisotropy in the bonding between atoms in different crystal planes. In the context of a tetragonal structure, the anisotropic shear factors A_1 and A_3 are expected to have values equal to unity for an isotropic crystal. Hence, any deviation from unity reflects the extent of elastic anisotropy. In Table 4, we present the calculated values of A_1 and A_3 for the title materials. The results indicate significant shear anisotropy along the {100} and {001} shear planes. This finding underscores the pronounced variation in bonding strengths and mechanical responses of atoms in different crystallographic directions.

(iv) In a tetragonal system, the crystal direction-dependent Young's modulus (E) and linear compressibility (β) can be expressed in the spherical coordinate system as follows [44]:

$$\begin{cases} \frac{1}{E} = (l_1^4 + l_2^4)S_{11} + l_3^4 S_{33} + 2l_1^2 l_2^2 S_{12} + 2(l_1^2 l_3^2 + 2l_2^2 l_3^2)S_{13} + (l_2^2 l_3^2 + l_1^2 l_3^2)S_{44} + l_1^2 l_2^2 S_{66} \\ \beta = (S_{11} + S_{12} + S_{13}) - (S_{11} + S_{12} - S_{13} - S_{33})l_3^2 \end{cases} \quad (22)$$

Here, l_1, l_2, and l_3 are the direction cosines, and S_{ij} are the components of the compliance matrix. An elastic modulus isotropic with respect to crystal directions in 3D is represented by a closed surface that assumes a perfect spherical configuration. This is because the elastic modulus is the same in all directions for an isotropic material, and a sphere is the only shape that has the same radius in all directions. Therefore, the degree of deviation of the shape of this closed surface from its spherical shape reflects the degree of anisotropy of the represented elastic modulus. Figure 5 show the 3D contours of E and β as well as their cross-sections (2D contours) in the (001), (010), and (001) crystalline planes for the considered compounds. As can be seen, the 3D representations (2D representations) of the Young's modulus deviate considerably from the spherical shape (circular form), indicating that this property is noticeably anisotropic for both studied compounds. In $CaRh_2P_2$ ($CaRh_2P_2$), the minimum value of E (E_{min}) is 184 GPa (94 GPa) along the [001] direction, and the maximum value (E_{max}) is 219 GPa (203 GPa) along the [110] direction. Similarly, the 3D-representations (2D-representations) of the linear compressibility of $CaRh_2P_2$ and $BaRh_2P_2$ deviate considerably from the spherical shape (circular form), indicating that this property is also noticeably anisotropic. In $CaRh_2P_2$ ($BaRh_2P_2$), the minimum value of β (β_{min}) is 0.0018 GPa^{-1} (0.0025 GPa^{-1}) along the [001] direction (along any direction in the (001) plane), and the maximum value (β_{max}) is 0.0024 GPa^{-1} (0.0060 GPa^{-1}) along any direction in the (001) plane (along the [001] direction) direction. This is consistent with the statement that has already been drawn from the elastic constants C_{11}, and C_{33}. The consistent difference between E_{max} (β_{max}) and E_{min} (β_{min}) indicates the strong anisotropy of the Young's modulus (linear compressibility) in the considered compounds.

3.3 Thermodynamic Properties

The thermodynamic characteristics of the materials under investigation were subjected to comprehensive analysis through the utilization of the quasi-harmonic Debye approximation [71], and executed using the specialized computational framework known as the Gibbs software [30]. Within the scope of this particular investigation, a thorough exploration was conducted into the temperature-dependent behavior of several key material physical parameters. These physical parameters encompass the lattice parameter, bulk modulus, thermal expansion coefficient, heat capacity, and Debye temperature. The temperature range scrutinized spanned from absolute zero up to 600 K, and this analysis was conducted under controlled pressures held at fixed values of 0, 4, 8, 12, and 16.

Figure 6a illustrates the change in the lattice parameter "*a*" with change in temperature at the fixed pressures 0, 4, 8, 12, and 16 GPa. The lattice parameter increases as the temperature rises, while in contrast, it decreases with increasing pressure, proving the contrasting effects of temperature and

Table 4 Calculated universal anisotropic index (A^U), percent anisotropy (A_{comp} and A_{shear}) and shear anisotropic factors (A_1 and A_2) for $BaRh_2 \times_2$ (X = P, As) compounds as well as the results of previous calculations for some isostructural compounds

Compound	A_{comp}	A_{shear}	A^U	$A_1 = A_{\{100\}}$	$A_3 = A_{\{001\}}$
$CaRh_2P_2$	0.026	0.080	0.086	1.110	1.350
$BaRh_2P_2$	0.031	0.072	0.840	0.790	1.740
$BaRu_2P_2$ [32]	0.097	0.105	1.399	0.789	1.909
$BaRu_2As_2$ [32]	0.071	0.076	0.980	0.976	1.626
$CaRu_2P_2$ [35]	-	-	0.730	-	-
$CaRu_2As_2$ [35]	-	-	0.620	-	-
YRu_2P_2 [42]	-	-	0.270	-	-

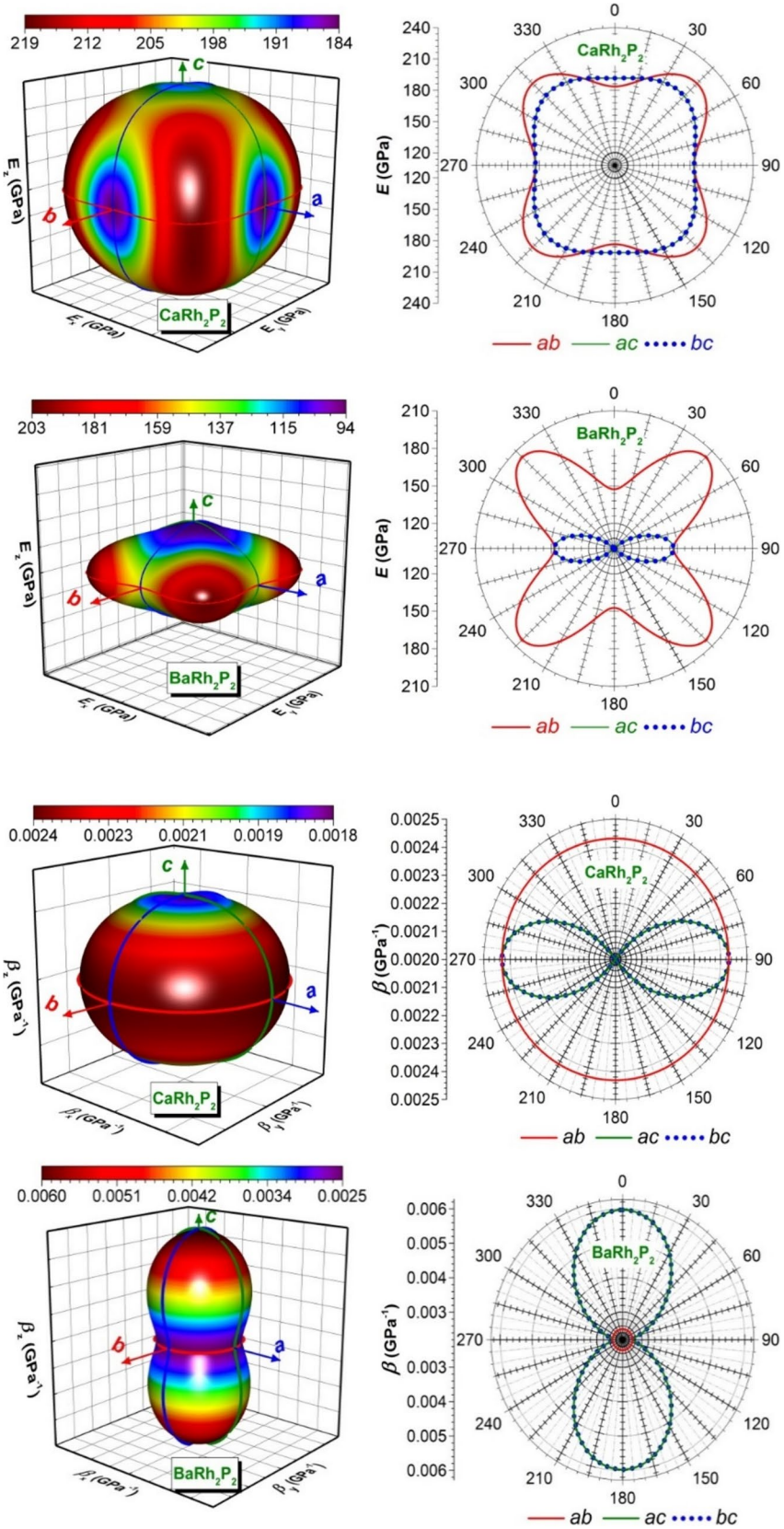

Fig. 5 Direction-dependent Young's modulus E and linear compressibility β as well as the corresponding cross-sections in the (100)/(010), (001) and planes for $CaRh_2P_2$ and $BaRh_2P_2$ crystals

pressure on the lattice parameter. Our computations indicate that at zero pressure and T = 300 K, the lattice parameter is 4.2698 Å for $CaRh_2P_2$, and 4.6112 Å for $BaRh_2P_2$.

Figure 6b illustrates the variation of the bulk modulus (B) as it responds to temperature alterations, all while being subjected to a series of unchanging pressures, namely 0, 4, 8, 12, and 16 GPa. Notably, the observed trend demonstrates a decline in the bulk modulus magnitude with the escalation of temperature. Furthermore, it becomes evident that an increase in pressure corresponds to an augmentation in the bulk modulus magnitude. Upon closer examination, it becomes evident that, under the conditions of zero pressure and a temperature of 300 K, the calculated bulk modulus values stand at 123.17 GPa for $CaRh_2P_2$ and 80.6 GPa for $BaRh_2P_2$. These numerical results distinctly indicate that $CaRh_2P_2$ exhibits a considerably greater resistance to deformation in comparison to $BaRh_2P_2$, implying a higher degree of structural rigidity and stability.

Thermal expansion (α), a phenomenon caused by the inherent mobility of the constituent atoms or molecules of a material, refers to the propensity of a substance to undergo volumetric expansion upon exposure to high temperatures. Figure 6c visually elucidates the nuanced trajectory of the coefficient of thermal expansion as a function of temperature and pressure changes. Notably, this diagram depicts a clear trend in which the coefficient of thermal expansion (α) experiences an accelerated increase as temperatures rises from zero to about 200 K. Beyond this temperature threshold, a more moderate and essentially linear progression characterizes his growth. Conversely, a noticeable decrease in the coefficient of thermal expansion is noticeable with increasing pressure, a trend evident in both composite materials. The coefficient of volumetric thermal expansion, evaluated at zero pressure and at a temperature of 300 K, amounts to $5.98636 \times 10^{-5} K^{-1}$ for $CaRh_2P_2$ and $6.36372 \times 10^{-5} K^{-1}$ for $BaRh_2P_2$, respectively.

Figure 6d and e shows the relationship between temperature and heat capacity, both at constant volume (C_V) and constant pressure (C_P), at the fixed pressures of 0, 4, 8, and 16 GPa. In the lower temperature steps, precisely covering the interval from 0 to 200 K, the values of C_V and C_P unquestionably follow a proportional relationship

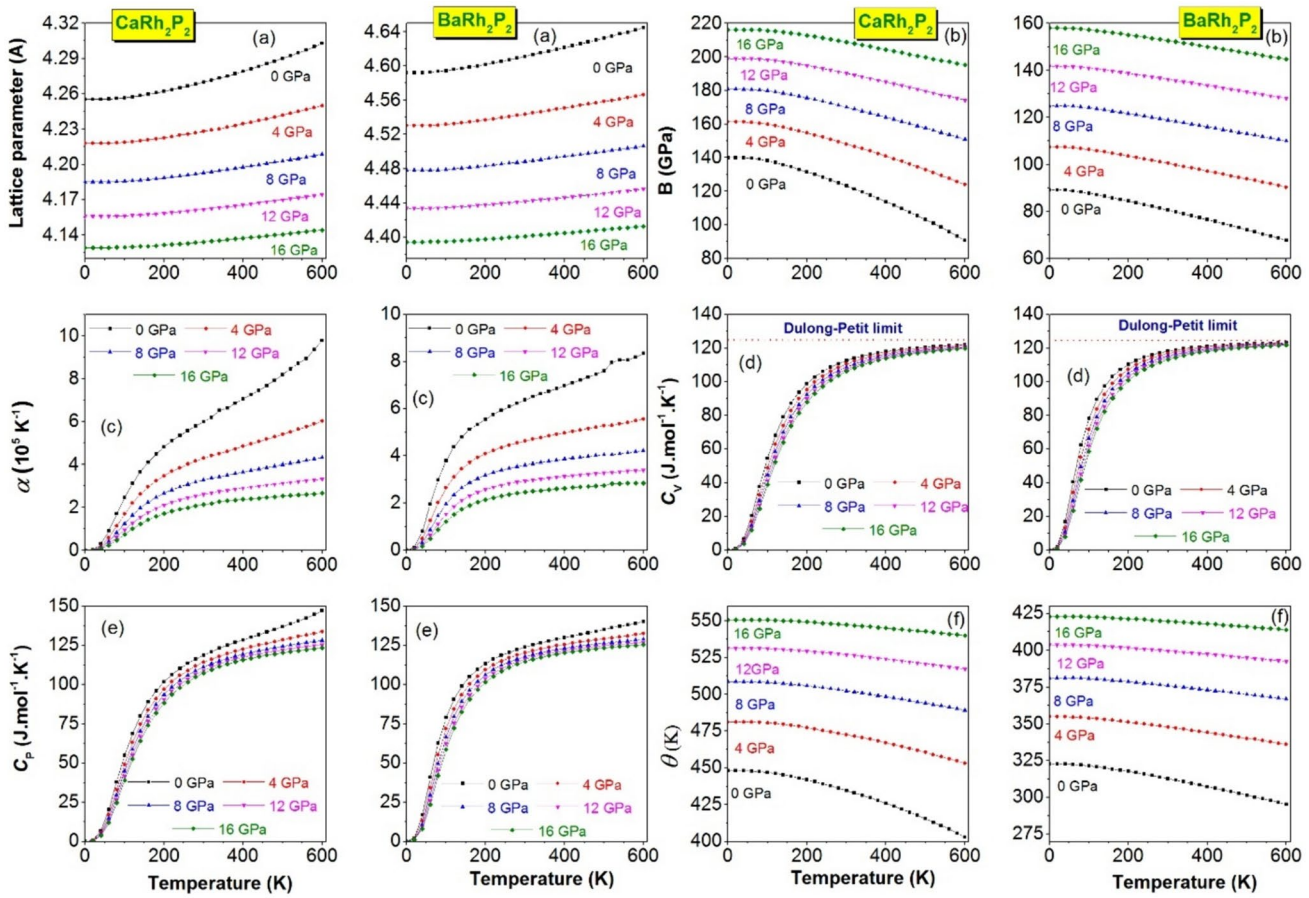

Fig. 6 Temperature dependence of the lattice parameter (**a**) bulk modulus; B (**b**), thermal expansion coefficient; α (**c**), heat capacity at constant volume; C_V (**d**) heat capacity at constant pressure; C_P (**d**) and Debye temperature; θ (**f**) of $CaRh_2P_2$ and $BaRh_2P_2$ compounds at fixed pressures of 0, 4, 8, 12 and 16 GPa

with the cubic power of temperature (T^3). With increasing temperature, the increase in C_V follows a gradual trajectory, gradually aligning with the eminent Dulong-Petit limit (1240.66 $J.mol^{-1}.K^{-1}$). In contrast, the C_P constantly progresses in a linear fashion as the temperature increases. It is important to note that C_V and C_P tend to decrease as pressure increases. At a perfect intersection of zero pressure and a fixed temperature of 300 K, the estimated value of C_V (C_P) add up to 112.54 $J.mol^{-1}.K^{-1}$ (118.76 $J.mol^{-1}.K^{-1}$) for $CaRh_2P_2$ and 118.19 $J.mol^{-1}.K^{-1}$ (123.98 $J.mol^{-1}.K^{-1}$) for $BaRh_2P_2$.

The temperature dependence of the Debye temperature (θ_D) for the studied compounds at fixed pressures of 0, 4, 8, 12 and 16 GPa is illustrated in Fig. 6f. θ_D remains practically constant below 100 K, but then decreases gradually with increasing temperature. With increasing pressure, θ_D shows a noticeable increase, from 448.1 K(322.6 K) at zero pressure to 550.8 K (423.1K) at 16 GPa for $CaRh_2P_2$ ($BaRh_2P_2$). This increase in θ_D with pressure is due to the increase in the velocities of elastic waves, which in turn is caused by the increase in the interatomic forces. At zero pressure and 300 K, the approximate value of θ_D is 250 K for $CaRh_2P_2$ and 280 K for $BaRh_2P_2$. These values are in good agreement with the corresponding values derived from the elastic constants, which provides further confirmation of the reliability of the obtained results.

4 Conclusion

The first-principles PP-PW method with the GGA-PBE exchange–correlation functional was used to calculate the effect of pressure on the structural, elastic, and thermodynamic properties of the tetragonal XRh_2P_2 (X = Ca, Ba) compounds. The main conclusions are as follows:

(i) The computed ground state structural parameters are in good agreement with the experimental counterparts. The values obtained for the interlayer P-P bond distance reveal that $BaRh_2P_2$ is superconducting, while $CaRh_2P_2$ is not superconducting.
(ii) The predicted values of the single-crystal elastic constants for the considered materials at zero-pressure as well as under hydrostatic pressure up to 18 GPa satisfy the mechanical stability conditions, and show high uniaxial elastic anisotropy.
(iii) Pugh's ratio, Cauchy pressure, and Poisson's ratio indicate that XRh_2P_2 (X = Ca, Ba) are ductile materials. The XRh_2P_2 (X = Ca, Ba) compounds are expected to resist to shear distortion in the <110> more than in the (100) plane.
(iv) The shear and bulk moduli (B, and G), Poisson's ratio (σ), and Young's modulus (E) increase with increasing pressure. The Vickers hardness, Debye temperature, sound wave velocity, melting temperature, and minimum thermal conductivity values were predicted in the pressure range from 0 to 18 GPa.
(v) The temperature-dependency of the lattice parameter, bulk modulus, Debye temperature, volume thermal expansion coefficient, and isobar and isochoric heat capacities at the fixed pressures of 0, 4, 8, 12, and 16 GPa were successfully determined via the quasi-harmonic Debye model.

To conclude, there are no experimental studies regarding the thermodynamic and elastic properties of the tetragonal XRh_2P_2 (X = Ca, Ba) compounds to be compared to our results. Therefore, we expect that this study will stimulate further theoretical and experimental research activities.

Acknowledgements The author S. Bin-Omran acknowledges the Researchers Supporting Project number RSP2024R82, King Saud University, Riyadh, Saudi Arabia.

Author Contributions Authors' contributions: M.S: Writing - original draft. M.R: Conceptualization, Formal analysis. A.B: Visualization, Writing - review, editing, Validation, Methodology. Y.I.B: Review, Editing. S.C: Prepared figures, Writing. S.B: Methodology. All authors carefully reviewed the manuscript in all its versions.

Funding This research was supported by Researchers Supporting Project Number (RSP2024R82), King Saud University, Riyadh, Saudi Arabia.

Data Availability No datasets were generated or analysed during the current study.

Declarations

Competing Interests The authors declare no competing interests.

References

1. Felt, U., Nowotny, H.: Striking gold in the 1990s: the discovery of high-temperature superconductivity and its impact on the science system. Sci. Technol. Hum. Values **17**(4), 506–531 (1992)
2. Sheahen, T.: Introduction to high-temperature superconductivity. Springer Science and Business Media (1994)
3. Steglich, F., Aarts, J., Bredl, C.D., Lieke, W., Meschede, D., Franz, W., Schäfer, H.: Superconductivity in the presence of strong pauli paramagnetism: $CeCu_2Si_2$. Phys. Rev. Lett. **43**(25), 1892 (1979)
4. Ronning, F., Kurita, N., Bauer, E.D., Scott, B.L., Park, T., Klimczuk, T., Thompson, J.D.: The first order phase transition and superconductivity in $BaNi_2As_2$ single crystals. J. Phys. Condens. Matter **20**(34), 342203 (2008)
5. Shein, I.R., Ivanovskii, A.L.: Electronic and structural properties of low-temperature superconductors and ternary pnictides ANi_2Pn_2 (A = Sr, Ba and P n = P, as). Phys. Rev. B **79**(5), 054510 (2009)
6. Bauer, E.D., Ronning, F., Scott, B.L., Thompson, J.D.: Superconductivity in $SrNi_2As_2$ single crystals. Phys. Rev. B **78**(17), 172504 (2008)
7. Trovarelli, O., Geibel, C., Mederle, S., Langhammer, C., Grosche, F.M., Gegenwart, P., Steglich, F.: $YbRh_2Si_2$: pronounced

non-fermi-liquid effects above a low-lying magnetic phase transition. Phys. Rev. Lett. **85**(3), 626 (2000)
8. Shelton, R.N., Braun, H.F., Musick, E.: Superconductivity and relative phase stability in 1: 2: 2 ternary transition metal silicides and germanides. Solid State Commun. **52**(9), 797–799 (1984)
9. Shein, I.R., Ivanovskii, A.L.: Structural, elastic, electronic and magnetic properties of $ThCr_2Si_2$ from first-principles calculations. Solid State Commun. **151**(17), 1165–1168 (2011)
10. Ban, Z., Sikirica, M.: The crystal structure of ternary silicides ThM_2Si_2 (M = cr, Mn, Fe, Co, Ni and Cu). Acta Crystallogr. A **18**(4), 594–599 (1965)
11. Just, G., Paufler, P.: On the coordination of $ThCr_2Si_2$ ($BaAl_4$-type compounds within the field of free parameters. J. Alloys. Compd. **232**(1–2), 1–25 (1996)
12. Salma, M.U., Rahman, M.A.: Physical properties of $ThCr_2Si_2$-type Rh-based compounds ARh_2Ge_2 (A = ca, Sr, Y and Ba): DFT based first-principles investigation. Int J. Mod. Phys. B **32**(32), 1850357 (2018)
13. Qin, M., Yang, C., Wang, Y., Yang, Z., Chen, P., Huang, F.: Synthesis, physical properties and electronic structure of $Sr_{1-x}La_xCu_2Pn_2$ (pn = P, as, sb). J. Solid State Chem. **187**, 323–327 (2012)
14. Braun, H.F., Engel, N., Parthé, E.: Polymorphism and superconductivity of $LaIr_2Si_2$. Phys. Rev. B. **28**(3), 1389 (1983)
15. Banu, I.S., Rajagopalan, M., Yousuf, M., Shenbagaraman, P.: Electronic and bonding properties of ANi_2P_2 (A = ca, Sr, Ba). J. Alloys Compd. **288**(1–2), 88–95 (1999)
16. Anand, V.K., Kim, H., Tanatar, M.A., Prozorov, R., Johnston, D.C.: Superconducting and normal-state properties of APd_2As_2 (A = ca, Sr, Ba) single crystals. Phys. Rev. B **87**(22), 224510 (2013)
17. Hoffmann, R., Zheng, C.: Making and breaking bonds in the solid state: The $ThCr_2Si_2$ structure. J. Phys. Chem. **89**(20), 4175–4181 (2002)
18. Berry, N., Capan, C., Seyfarth, G., Bianchi, A.D., Ziller, J., Fisk, Z.: Superconductivity without Fe or Ni in the phosphides $BaIr_2P_2$ and $BaRh_2P_2$. Phys. Rev. B **79**(18), 180502 (2009)
19. Foroozani, N., Lim, J., Schilling, J., Fotovat, R., Zheng, C., Hoffmann, R.: Hydrostatic high-pressure studies to 25 GPa on the model superconducting pnictide $LaRu_2P_2$. J. Phy. Conf. Ser. **500**(3), 032007 (2014). IOP Publishing
20. Anand, V.K., Kim, H., Tanatar, M.A., Prozorov, R., Johnston, D.C.: Superconductivity and physical properties of $CaPd_2Ge_2$ single crystals. J. Phys. Condens. Matter **26**(40), 405702 (2014)
21. Mine, T., Yanagi, H., Kamiya, T., Kamihara, Y., Hirano, M., Hosono, H.: Nickel-based phosphide superconductor with infinite-layer structure, $BaNi_2P_2$. Solid State Commun. **147**(3–4), 111–113 (2008)
22. Vališka, M., Pospíšil, J., Prokleška, J., Diviš, M., Rudajevová, A., Sechovský, V.: Superconductivity in the YIr_2Si_2 and $LaIr_2Si_2$ polymorphs. J. Phys. Soc. Jpn. **81**(10), 104715 (2012)
23. Hirai, D., Takayama, T., Higashinaka, R., Aruga-Katori, H., Takagi, H.: Superconductivity in layered pnictides $BaRh_2P_2$ and $BaIr_2P_2$. J. Phys. Soc. Jpn. **78**(2), 023706–023706 (2009)
24. Clark, S.J., Segall, M.D., Pickard, C.J., Hasnip, P.J., Probert, M.I., Refson, K., Payne, M.C.: First principles methods using CASTEP. Z. Kristallogr. Cryst. Mater. **220**(5–6), 567–570 (2005)
25. Perdew, J.P., Ruzsinszky, A., Csonka, G.I., Vydrov, O.A., Scuseria, G.E., Constantin, L.A., Burke, K.: Restoring the density-gradient expansion for exchange in solids and surfaces. Phys. Rev. Lett. **100**(13), 136406 (2008)
26. Vanderbilt, D.: Soft self-consistent pseudopotentials in a generalized eigenvalue formalism. Phys. Rev. B **41**(11), 7892 (1990)
27. Monkhorst, H.J., Pack, J.D.: Special points for Brillouin-Zone integrations. Phys. Rev. B **13**(12), 5188 (1976)
28. Fischer, T.H., Almlof, J.: General methods for geometry and wave function optimization. J. Phys. Chem. **96**(24), 9768–9774 (1992)
29. Kang, J., Lee, E.C., Chang, K.J.: First-principles study of the structural phase transformation of hafnia under pressure. Phys. Rev. B. **68**(5), 054106 (2003)
30. Blanco, M.A., Francisco, E., Luana, V.: GIBBS: Isothermal-isobaric thermodynamics of solids from energy curves using a quasi-harmonic debye model. Comput. Phys. Commun. **158**(1), 57–72 (2004)
31. Wurth, A., Johrendt, D., Mewis, A., Huhnt, C., Michels, G., Roepke, M., Schlabitz, W.: Über Den Einfluß Von Temperatur, Druck und substitution auf die Kristallstruktur Von ARh_2P_2 (A = ca, Sr, Eu, Ba). Z. Anorg. Allg. Chem. **623**(9), 1418–1424 (1997)
32. Radjai, M., Bouhemadou, A.: Physical properties of $BaRu_2X_2$ (X = P, as) superconducting compound sunder pressure effects: Ab initio study. Physica C. (Amsterdam, Neth.) **604**, 1354176 (2023)
33. Wenski, G., Mewis, A.: $BaAl_4$-Strukturvarianten bei ARu_2X_2 (A = ca, Sr, Ba, Eu; X = P, as) und APt_2P_{2-x} (A = ca, Eu)/$BaAl_4$-Denvative structures of ARu_2X_2 (A = ca, Sr, Ba. Eu; X = P, as) and of APt_2P_{2-x} (A = ca, Eu). Z. Naturforsch. B **41**(1), 38–43 (1986)
34. Sasmal, K., Lv, B., Lorenz, B., Guloy, A.M., Chen, F., Xue, Y.Y., Chu, C.W.: Superconducting Fe-based compounds ($A_{1-x}Sr_x$) Fe_2As_2 with A = K and Cs with transition temperatures up to 37 K. Phys. Rev. Lett. **101**(10), 107007 (2008)
35. Radjai, M., Bouhemadou, A., Bitam, T.: First-principles investigation of the structural, elastic and thermodynamic properties of $CaRu_2X_2$ (X = P, As) under pressure. J. Supercond. Novel. Magn. **35**(9), 2531–2544 (2022)
36. Jeitschko, W., Glaum, R., Boonk, L.: Superconducting $LaRu_2P_2$ and other alkaline earth and rare earth metal ruthenium and osmium phosphides and arsenides with $ThCr_2Si_2$ structure. J. Solid State Chem. **69**(1), 93–100 (1987)
37. Birch, F.: Finite elastic strain of cubic crystals. Phys. Rev. **71**(11), 809 (1947)
38. Vinet, P., et al.: Compressibility of solids. J. Geophys. Res. Solid Earth **92**(B9), 9319–9325 (1987)
39. Radjai, M., Maouche, D., Guechi, N., Cheddadi, S., Kechidi, Z.: Investigation of structural and elastic properties of monoclinic Ba_2P_7X (X = Cl, Br, I) Zintl Salts compounds. arXiv preprint arXiv:1910.00915 (2019)
40. Chaba Mouna, S., Radjai, M., Bouhemadou, A., Houatis, D., Allali, D., Essaoud, S., Bin-Omran, S.: Structural, elastic, and thermodynamic properties of $BaXCl_3$ (X = Li, Na) perovskites under pressure effect: ab initio exploration. Phys. Scr. **98**(6), 065949 (2023)
41. Westbrook, J.H.: Intermetallic compounds, structural applications of, Vol. 3 Wiley (2000)
42. Rehman, J.U., Usman, M., Tahir, M.B., Hussain, A., Rashid, M.: Investigation of structural, electronics, optical, mechanical and thermodynamic properties of YRu_2P_2 compound for superconducting application. J. Supercond. Novel Magn. **34**(12), 3089–3097 (2021)
43. Hadi, M.A., Ali, M.S., Naqib, S.H., Islam, A.K.: New ternary superconducting compound $LaRu_2As_2$: physical properties from density functional theory calculations. Chin. Phys. B **26**(3), 037103 (2017)
44. Nye, J.F.: Physical properties of crystals: their representation by tensors and matrices. Oxford University Press (1985)
45. Alouani, M., Albers, R.C., Methfessel, M.: Calculated elastic constants and structural properties of Mo and $MoSi_2$. Phys. Rev. B **43**(8), 6500 (1991)
46. Born, M., Huang, K., Lax, M.: Dynamical theory of crystal lattices. Am. J. Phys. **23**(7), 474–474 (1955)
47. Wu, Z.J., Zhao, E.J., Xiang, H.P., Hao, X.F., Liu, X.J., Meng, J.: Crystal structures and elastic properties of superhard IrN_2 and IrN_3 from first principles. Phys. Rev. B **76**(5), 054115 (2007)
48. Sin'Ko, G.V., Smirnov, N.A.: Ab initio calculations of elastic constants and thermodynamic properties of bcc, fcc, and hcp Al crystals under pressure. J. Phys. Condens. Matter **14**(29), 6989 (2002)
49. Reuss, A., Angew, Z.: Math. Mech. **9**, 5566 (1929)

50. Voigt, W.: Lehrbuch der Kristallphysik (Leipzig: Teubner). Adv. Earth Science **1**, 1–978 (1928)
51. Hill, R.: The elastic behaviour of a crystalline aggregate. Proc. Phys. Soc. A **65**(5), 349 (1952)
52. Bedjaoui, A., Bouhemadou, A., Bin-Omran, S.: Structural, elastic and thermodynamic properties of tetragonal and orthorhombic polymorphs of Sr_2GeN_2: an ab initio investigation. High Press. Res. **36**(2), 198–219 (2016)
53. Chen, X.Q., Niu, H., Franchini, C., Li, D., Li, Y.: Hardness of T-carbon: density functional theory calculations. Phys. Rev. B **84**(12), 121405 (2011)
54. Chen, X.Q., Niu, H., Li, D., Li, Y.: Modeling hardness of polycrystalline materials and bulk metallic glasses. Intermetallics **19**(9), 1275–1281 (2011)
55. Pugh, S.F.: XCII. Relations between the elastic moduli and the plastic properties of polycrystalline pure metals. Lond. Edinb. Dublin Philos. Mag. & J. Sci. **45**(367), 823–843 (1954)
56. Radjai, M., Bouhemadou, A., Bin-Omran, S.: Ab initio study of pressure dependence of the structural, elastic and thermodynamic properties of $AlXY_3$ (X = B, C). Phase Transit. **96**(1), 1–15 (2023)
57. Anderson, O.L.: A simplified method for calculating the Debye temperature from elastic constants. J. Phys. Chem. Solids **24**(7), 909–917 (1963)
58. Radjai, M., Bouhemadou, A., Maouche, D.: Structurlastic, electronic and optical properties of the half-Heusler ScPtSb and YPtSb compounds under pressure. arXiv preprint arXiv:2112099 40 (2021)
59. Kanchana, V., Vaitheeswaran, G., Svane, A., Delin, A.: First-principles study of elastic properties of CeO_2, ThO_2 and PoO_2. J. Phys. Condens. Matter **18**(42), 9615 (2006)
60. Karaca, E., Karadağ, S., Tütüncü, H.M., Srivastava, G.P., Uğur, Ş: First-principles investigation of superconductivity in the body-centred tetragonal. Phil. Mag. **96**(19), 2059–2073 (2016)
61. Clarke, D.R.: Materials selection guidelines for low thermal conductivity thermal barrier coatings. Surf. Coat. Technol. **163**, 67–74 (2003)
62. Li, J., Van Vliet, K.J., Zhu, T., Yip, S., Suresh, S.: Atomistic mechanisms governing elastic limit and incipient plasticity in crystals. Nature **418**(6895), 307–310 (2002)
63. Lloveras, P., Castán, T., Porta, M., Planes, A., Saxena, A.: Influence of elastic anisotropy on structural nanoscale textures. Phys. Rev. Lett. **100**(16), 165707 (2008)
64. Tvergaard, V., Hutchinson, J.W.: Microcracking in ceramics induced by thermal expansion or elastic anisotropy. J. Am. Ceram. Soc. **71**(3), 157–166 (1988)
65. Huang, B., Duan, Y.H., Hu, W.C., Sun, Y., Chen, S.: Structural, anisotropic elastic and thermal properties of MB (M = Ti, Zr and Hf) monoborides. Ceram. Int. **41**(5), 6831–6843 (2015)
66. Li, R.Y., Duan, Y.H.: Anisotropic elastic properties of MB (M = Cr, Mo, W) monoborides: a first-principles investigation. Phil. Mag. **96**(10), 972–990 (2016)
67. Ozisik, H.B., Colakoglu, K., Deligoz, E.: First-principles study of structural and mechanical properties of AgB_2 and AuB_2 compounds under pressure. Comput. Mater. Sci. **51**(1), 83–90 (2012)
68. Radjai, M., Guechi, N., Maouche, D.: An ab initio study of structurlastic and electronic properties of hexagonal MAuGe (M = Lu, Sc) compounds. arXiv preprint arXiv:2103.15579 (2021)
69. Mo, Y., Pang, M., Yang, W., Zhan, Y.: Effects of alloying elements on structural, electronic and mechanical properties of $AlSc_2$ by first-principles calculations. Comput. Mater. Sci. **69**, 160–167 (2013)
70. Wu, M.M., Wen, L., Tang, B.Y., Peng, L.M., Ding, W.J.: First-principles study of elastic and electronic properties of $MgZn_2$ and $ScZn_2$ phases in Mg–Sc–Zn alloy. J. Alloys Compd. **506**(1), 412–417 (2010)
71. Blanco, M.A., Pendás, A.M., Francisco, E., Recio, J.M., Franco, R.: Thermodynamical properties of solids from microscopic theory: applications to MgF_2 and Al_2O_3. J. Mol. Struct. (Thoechem) **368**, 245–255 (1996)